Nickel Hydroxide Tubes

$Ni(OH)_2$ Tubes with Mesoscale Dimensions as Positive-Electrode Materials of Alkaline Rechargeable Batteries**

Feng-Shi Cai, Guo-Ying Zhang, Jun Chen, Xing-Long Gou, Hua-Kun Liu, and Shi-Xue Dou*

Rechargeable batteries are becoming more and more important in everyday life, especially in consumer electronic devices such as cellular telephones, notebook computers, compact camcorders, and electric vehicles.[1–3] The nickel hydroxide/nickel oxyhydroxide couple $Ni(OH)_2/NiOOH$ is the primary redox system used as the positive electrode of alkaline rechargeable batteries including nickel/cadmium (Ni/Cd), nickel/iron (Ni/Fe), nickel/metal hydride (Ni/MH), and nickel/zinc (Ni/Zn).[4,5] These batteries are usually positive-

[*] Dr. F.-S. Cai, Dr. G.-Y. Zhang, Prof. Dr. J. Chen, Dr. X.-L. Gou
Institute of New Energy Materials Chemistry
Nankai University, Tianjin 300071
and National Center for Nanoscience and Nanotechnology
Beijing 100084 (P. R. China)
Fax: (+86) 22-2350-9118
E-mail: chenabc@nankai.edu.cn
Prof. H.-K. Liu, Prof. Dr. S.-X. Dou
Institute for Superconducting & Electronic Materials
University of Wollongong, NSW 2522 (Australia)

[**] This work was supported by the National NSFC (20325102), TCTPF (200248)—Key Project (104055), and 973 Program (2003CB211800 and 2003CB). F.S.C. and G.Y.Z. contributed equally to this work. We thank two referees for pertinent comments.

  DOI: 10.1002/ange.200460053

electrode-limited for reasons of proper recombination reactions and battery safety. It follows that increasing the energy density of the nickel hydroxide electrode is essential for raising the energy density of such batteries.

The reversible nickel electrode reaction may be briefly described by Equation (1).

$$\beta\text{-Ni(OH)}_2 + OH^- \rightleftharpoons \beta\text{-NiOOH} + H_2O + e^- \quad (1)$$

That is, nickel hydroxide $Ni(OH)_2$ is oxidized on charging to nickel oxyhydroxide (NiOOH). Thus, one mole of $Ni(OH)_2$ (92.7 g) can theoretically yield a capacity of 289(26800/92.7) mA h g^{-1}. However, the charge/discharge reactions which take place in the nickel hydroxide electrode are much more complex. Four phases are reported to be produced over the lifetime of a nickel hydroxide electrode, namely, β-$Ni(OH)_2$, β-NiOOH, γ-NiOOH, and α-$Ni(OH)_2$.[6,7] α-$Ni(OH)_2$ can also be oxidized to γ-NiOOH at a lower potential than the corresponding oxidation state compared with β-$Ni(OH)_2$, with a higher discharge capacity than β-$Ni(OH)_2$/β-NiOOH, since the nickel oxidation state in γ-NiOOH is known to exceed 3 because of Ni^{4+} defects.[8] The formation of these phases is associated with volume expansion or swelling of the nickel hydroxide electrode, which interferes with effective contact between particles of the active material, and this increases the resistance of the electrode reaction, especially at high-rate or high-temperature charge/discharge.[9] To improve the characteristics of the nickel hydroxide electrode, much work has focused on the development of spherical $Ni(OH)_2$ powder and related composite materials.[10–14] Nickel hydroxide particles with nanostructural multiphase exhibit superior electrochemical behavior and higher proton diffusion coefficients.[15,16] On the one hand, spherical nickel hydroxide powder, which suppresses the development of inner-pore volume, makes it possible to increase the density of the active material itself. On the other hand, the core of spherical nickel hydroxide powder is still inactive at high-rate and high-temperature charge/discharge due to the diffusion barrier.

Recently, single-crystal $Ni(OH)_2$ nanorods[17] and β-$Ni(OH)_2$ nanosheets[18] have been prepared by the hydrothermal method. However, no attempt has been made to fabricate $Ni(OH)_2$ micro- and/or nanotubes and test their electrochemical activity. Here we report that $Ni(OH)_2$ tubes with mesoscale dimensions, produced by chemical deposition of nickel ions and ammonia within anodic alumina membranes, have superior capacity and good cycling reversibility, and are promising positive-electrode materials for alkaline rechargeable batteries.

$Ni(OH)_2$ tubes were synthesized by a template method,[19–22] as shown schematically in Figure 1. The preparation process mainly involves 1) impregnating nickel ions in the pore walls of the alumina template; 2) dripping ammonia solution through the alumina membrane to precipitate nickel hydroxide; 3) dissolving the alumina membrane in NaOH solution to obtain tube bundles.

The homogeneity and crystallinity of the product was examined by powder XRD (Figure 2). All the diffraction peaks can be indexed as a hexagonal β-$Ni(OH)_2$ structure

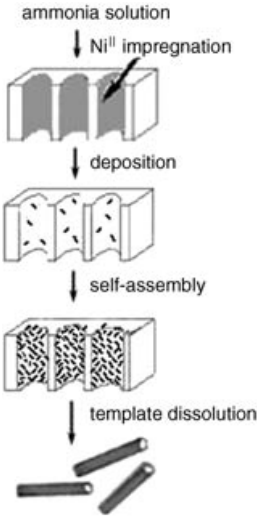

Figure 1. Schematic diagram showing the template preparation of $Ni(OH)_2$ tubes.

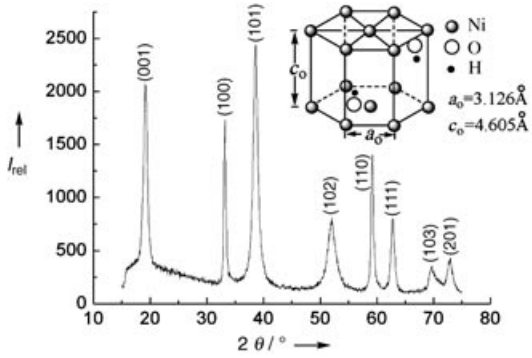

Figure 2. XRD pattern of the as-prepared β-$Ni(OH)_2$.

with the lattice constants $a = 3.127$ Å and $c = 4.606$ Å, in good agreement with that of the standard values (ICDD-JCPDS card No. 14-0117). The broadening of peaks in the XRD pattern indicates that the component crystallites are of nanoscale character. No peaks from other phases were found, that is, the as-synthesized β-$Ni(OH)_2$ is of high purity. The contents of Ni and Al in the product, analyzed by inductively coupled plasma (ICP) emission spectroscopy (Model P-5200 from Hitachi), were 62 and 0.1 %, respectively, that is, traces of alumina remain.

Figure 3 shows SEM images of the as-prepared sample at different magnifications. Figure 3a is an overall view of the product, from which it can be seen that a large quantity of filament bundles were obtained. The length of the bundles is approximately 60 μm, which corresponds to the thickness of the template membrane employed in the synthesis process. Figure 3b shows an SEM image of one bundle at a higher magnification. This shows that the $Ni(OH)_2$ tubes are arranged roughly parallel to one another with a smooth-surface alignment. This might be due to the remaining trace of the alumina matrix rather than a kind of self-organization. Figure 3c is a typical SEM image with end-on view, showing the open ends of a tube bundle. The tubes are not all 200 nm

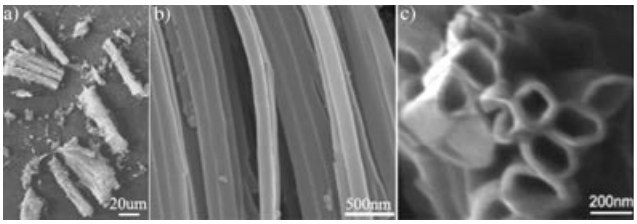

Figure 3. Typical SEM images of as-synthesized β-$Ni(OH)_2$. a) Overall view at low magnification. b) Walls of the tube bundles. c) Tube-bundle tips at high magnification.

in diameter, because of the pore-diameter distribution of the template around 200 nm. The tubes are cylinders with a wall thickness of 20–30 nm.

To further understand the detailed structure of the tubes, TEM and HRTEM were performed (Figure 4). Figure 4a is

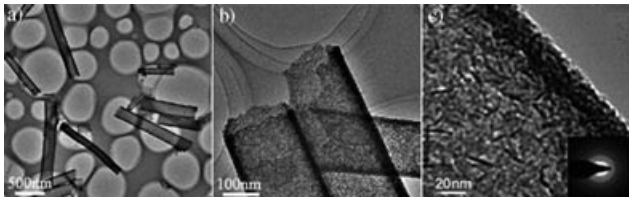

Figure 4. Representative TEM (a, b) and HRTEM (c) images of the as-prepared $Ni(OH)_2$ tubes. The inset in c) is the corresponding electron diffraction pattern.

the TEM image of a group of $Ni(OH)_2$ tubes scattered on the copper mesh. The central parts of the mesostructures are bright in contrast to their edges, confirming their hollow-tube nature. However, the tubes are only several micrometers long, much shorter than those observed in SEM images (ca. 60 μm). This phenomenon arises from the strong supersonic vibrations prior to the sample preparation for TEM analysis, that is, the long tubes were broken into shorter ones. The open-ended walls surrounding the central hollow core with an average outer diameter of 200 nm and a smooth surface are clearly visible in the TEM image of Figure 4b. The wall is complete and is composed of an array of needlelike and multilayered nanoparticles (Figure 4c). This was confirmed by the electron diffraction pattern of the tube (inset of Figure 4c), which shows the coexistence of nanocrystallites and amorphous structures. This result indicates that the crystallites have no preferred orientation. The mechanism of formation presumably resembles that of the noble-metal nanoparticle nanotubes reported by Rubinstein et al.[22] Note that under our synthesis conditions, the homogeneity of the $Ni(OH)_2$ tubes is high (> 98% based on the SEM and TEM observations). Therefore, the lengths and diameters of the tubes are definitely of mesoscale dimensions.

Figure 5 shows the cyclic voltammograms of the two spherical-powder and tube $Ni(OH)_2$ electrodes in the first cycle. Similarly shaped voltammograms were also obtained for five-potential cycling. Reversible peaks are observed for the spherical-powder and tube electrodes, but their characteristics are different. The features of the voltammograms are

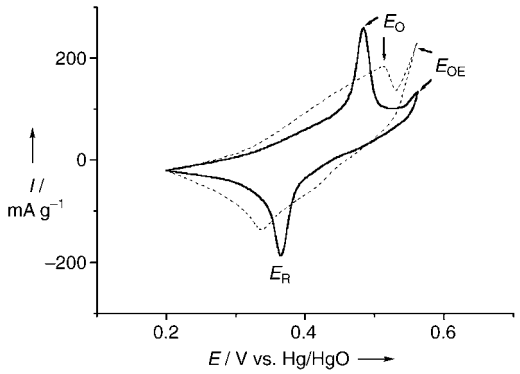

Figure 5. Cyclic voltammograms of $Ni(OH)_2$ tube (solid line) and spherical-powder (dotted line) electrodes at 20 °C and a scan rate of 0.5 mV s^{-1}.

summarized in Table 1: 1) When the electrodes were scanned cathodically, two peaks, for the oxidation potential E_O and oxygen-evolution potential E_{OE}, appeared; during the following anodic polarization, only one peak was observed, which was assigned to the reduction potential E_R. 2) The difference $E_O - E_R$ between the oxidation potential and the reduction potential is taken as a measure of the reversibility of the electrode reaction. The smaller this value, the more reversible the electrode reaction. 3) The intensities of E_O and E_R for the tube electrode were much larger than those of the spherical-powder electrode, that is, the energy density in the tube electrode is higher. 4) The difference between the oxygen-evolution potential and the oxidation potential $E_{OE} - E_O$, is also an important parameter for judging the performance of the nickel electrode. The value of $E_{OE} - E_O$ increased from 25 mV for the spherical-powder electrode to 77 mV for the tube electrode. This allows the tube electrode to be charged fully (i.e., complete oxidation of Ni^{2+} to Ni^{3+}) before oxygen evolution. Consequently, it demonstrates that the tube electrode exhibits much better electrochemical-cyclic properties than the spherical-powder electrode.

Table 1: Reduction potential E_R, oxidation potential E_O, oxygen-evolution potential E_{OE}, $E_O - E_R$, and $E_{OE} - E_O$ for the nickel hydroxide tube and spherical-powder electrodes at 20 °C.

Electrode	Potentials [mV]				
	E_R	E_O	E_{OE}	$E_O - E_R$	$E_{OE} - E_O$
Tube	365	485	562	120	77
Spherical powder	335	515	540	180	25

Figure 6 shows the charge–discharge curves of the tube and spherical-powder electrodes in the tenth cycle. The discharge curve of the tube electrode displays a higher discharge voltage and a longer plateau than that of the spherical-powder electrode, while its charge curve has a lower plateau. The highest discharge capacity of 315 mA h g^{-1} for the tube electrode, achieved at 50 mA g^{-1} and 20 °C, illustrates that in addition to the phase transformation of β-$Ni(OH)_2$ to β-NiOOH, partial formation of γ-NiOOH occurred.

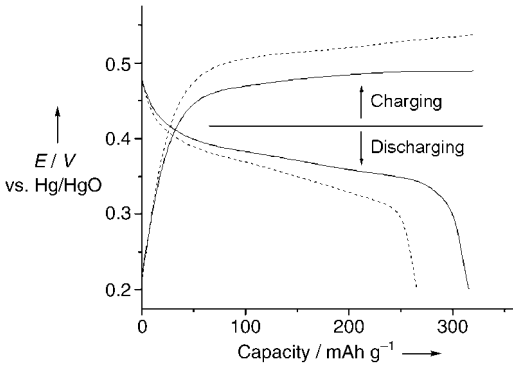

Figure 6. Charge/discharge curves as a function of capacity for nickel hydroxide tube (solid line) and spherical-powder (dotted line) electrodes at 20 °C.

Table 2 summarizes the effect of the working temperature and the discharge current density on the electrode capacity. At 20 °C and 150 mA g^{-1}, the tube electrode still retained 265 mA h g^{-1}, corresponding to about 84.1 % of the electrode capacity at 50 mA g^{-1}, while the spherical-powder electrode only showed 203 mA h g^{-1} (about 76.6 % of its capacity at 50 mA g^{-1}). Furthermore, it can also be seen that as the working temperature increases, the tube electrode has much higher capacities than the spherical-powder electrode. The tube electrode shows improved high-rate and high-temperature discharge ability due to the faster diffusion processes in the hollow tubes than in the dense spherical powder. This feature is critical for alkaline rechargeable batteries for high-power output at high temperatures.

Table 2: Effect of temperature and discharge current density on the discharge capacity of nickel hydroxide tube and spherical-powder electrodes.

Electrode	T [°C]	Current density [mA g^{-1}]	Discharge capacity [mA h g^{-1}]
Tube	20	50	315
		100	289
		150	265
	40	50	281
		100	257
		150	232
	60	50	251
		100	229
		150	205
Spherical powder	20	50	265
		100	235
		150	203
	40	50	233
		100	182
		150	154
	60	50	198
		100	155
		150	123

After a preliminary test of 50 charging/discharging cycles at 150 mA g^{-1} with 100 % depth of charge and discharge, the capacity of the tube electrode decreased by only about 4 %, that is, an average capacity fading of 0.2 mA h g^{-1} per cycle. Therefore, the hollow structure of the nickel hydroxide tube, which allows diffusion and oxidation/reduction to occur easily, contributes to superior capacity, reversibility, high-rate discharge, high-temperature performance, and cycling stability.

In summary, $Ni(OH)_2$ tubes prepared by a template method under ambient conditions can be used as the positive-electrode materials of alkaline rechargeable batteries showing important advantages in terms of capacity, high-rate discharge, and high-temperature performance.

Experimental Section

Anodic aluminum oxide membranes (Whatman, Φ47 mm with 0.2 μm pores and 60 μm thickness) were used as the templates. $NiCl_2{\cdot}6H_2O$, ammonia, and other reagents were all of analytical grade and used without further purification.

The $Ni(OH)_2$ tubes were prepared by chemical deposition within the alumina membranes. In a typical synthesis, an alumina template was gently immersed in 0.4 M aqueous solutions of $NiCl_2{\cdot}6H_2O$ for 30 min to fully impregnate the pore walls of the membrane with nickel ions. After removing the alumina membrane from the nickel solution, 2 M ammonia was slowly dripped onto it, so that the ammonia solution penetrated the template slowly under gravity and adhesive driving force. The white membrane gradually took on the light green color of nickel hydroxide. This solution filling and nickel hydroxide precipitation procedure was repeated several times at regular intervals to form tubes in the template pores. After five cycles, the membrane was rinsed with deionized water several times, and dissolved by 2 M NaOH solution. Then the solid was collected by filtration, washed with deionized water and absolute ethanol, and dried at 60 °C in vacuum for 2 h to obtain the product. The precipitation reaction of the nickel hydroxide can be expressed as Equation (2).

$$NiCl_2 \cdot 6H_2O + 2NH_4OH \rightarrow Ni(OH)_2 + 2NH_4Cl + 6H_2O \qquad (2)$$

The as-prepared samples were characterized by powder XRD (Rigaku INT-2000 X-ray generator, $Cu_{K\alpha}$ radiation), SEM (Philips XL-30, 20 kV), TEM, and high-resolution TEM (HRTEM; Philips Tecnai F20, 200 kV).

Nickel hydroxide electrodes were prepared by inserting an active paste into a nickel foam substrate. A paste containing 85 wt % nickel hydroxide tubes or spherical powder (Tanaka Chemical, Japan), 10 wt % carbon black, and 5 wt % polytetrafluoroethylene (PTFE) was used. The electrode was dried at 80 °C for 1 h and cut into a disk (1.2 × 1.2 cm), which was pressed at a pressure of 100 kg cm^{-2} to a thickness of 0.4 mm. Then the electrode was spot-welded to a nickel sheet for electrical connection. Electrochemical performance was measured with a Solartron SI 1260 Potentionstat Analyzer with 1287 Interface and an Arbin charge/discharge unit at controlled temperatures in an electrochemical cell, which contained the nickel hydroxide working electrode, a metal hydride electrode, a Hg/HgO reference electrode, and 6 M KOH solution as the electrolyte. The discharge capacity of the nickel hydroxide in the positive electrode was based on the amount of active material ($Ni(OH)_2$) excluding the weight of carbon black and PTFE in the electrode. The discharge capacity of each electrode was expressed in mA h per gram of active material.

Received: March 19, 2004 [Z460053]

Keywords: electrochemistry · nanotubes · nickel · rechargeable batteries · template synthesis

[1] S. R. Ovshinsky, M. A. Fetcenko, J. Ross, *Science* **1993**, *260*, 176.
[2] M. S. Dresselhaus, I. L. Thomas, *Nature* **2001**, *414*, 332.
[3] J. M. Tarascon, M. Armand, *Nature* **2001**, *414*, 359.
[4] J. McBreen in *Modern Aspects of Electrochemistry*, *Vol. 21* (Eds.: R. E. White, J. O'M. Bockris, B. E. Conway), Plenum, New York, **1990**, p. 29.
[5] D. Linden, *Handbook of Batteries*, 3rd ed., McGraw-Hill, New York, **2002**.
[6] H. Bode, K. Dehmelt, J. Witte, *Electrochim. Acta* **1966**, *11*, 1079.
[7] G. Halpert in *Nickel Hydroxide Electrodes*, *Vols. 90–94* (Eds.: D. A. Corrigan, A. H. Zimmerman), The Electrochemistry Society, Pennington, NJ, **1990**, p. 1.
[8] R. Barnard, C. F. Randell, F. L. Tye, *J. Appl. Electrochem.* **1980**, *10*, 109.
[9] D. Singh, *J. Electrochem. Soc.* **1998**, *145*, 116.
[10] M. Oshitani, M. Watada, T. Tanaka, T. Iida in *Hydrogen and Metal Hydride Batteries*, *Vol. 94* (Eds.: P. D. Bennett, T. Sakai), The Electrochemistry Society, Pennington, NJ, **1994**, p. 303.
[11] J. Chen, D. H. Bradhurst, S. X. Dou, H. K. Liu, *J. Electrochem. Soc.* **1999**, *146*, 3606.
[12] B. Liu, X. Y. Wang, H. T. Yuan, Y. S. Zhang, D. Y. Song, Z. X. Zhou, *J. Appl. Electrochem.* **1999**, *29*, 855.
[13] A. M. Fojas, E. Murphy, P. Stroeve, *Ind. Eng. Chem. Res.* **2002**, *41*, 2662.
[14] I. Zhitomirsky, *J. Appl. Electrochem.* **2004**, *34*, 235.
[15] E. David, J. Alvin, R. Peter, T. Xiao, *J. Power Sources* **1997**, *65*, 231.
[16] X. Wang, H. Luo, P. V. Parkhutik, A. C. Millan, E. Matveeva, *J. Power Sources* **2003**, *115*, 153.
[17] M. Keitaro, K. Takashi, T. Akira, *Adv. Mater.* **2002**, *14*, 1216.
[18] Z. H. Liang, Y. J. Zhou, X. L. Hu, *J. Phys. Chem. B* **2004**, *108*, 3488.
[19] C. R. Martin, *Science* **1994**, *266*, 1961.
[20] E. D. Sone, E. R. Zubarev, S. I. Stupp, *Angew. Chem.* **2002**, *114*, 1781; *Angew. Chem. Int. Ed.* **2002**, *41*, 1706.
[21] F. Schüth, *Angew. Chem.* **2003**, *115*, 3730; *Angew. Chem. Int. Ed.* **2003**, *42*, 3604.
[22] M. Lahav, T. Sehayek, A. Vaskeich, I. Rubinstein, *Angew. Chem.* **2003**, *42*, 5734; *Angew. Chem. Int. Ed.* **2003**, *42*, 5576.

